




# Synthesis microwave-assisted: fast method to obtain lithium-doped sodium titanate

A. D. Melo<sup>1</sup>, J. P. da Silva<sup>1</sup>, F. X. Nobre<sup>2</sup>, S. Costa<sup>3</sup>, J. C. C. Sales Jr<sup>1</sup>, J. Anglada-Rivera<sup>2</sup>, F. Guerrero<sup>3</sup>, M. M. da S. Paula<sup>3</sup>, R. F. B. de Souza<sup>4</sup>, R. Peña-García<sup>5,6</sup>, L. Aguilera<sup>7</sup>, and Y. Leyet<sup>1,3,\*</sup> 

<sup>1</sup>Departamento de Engenharia de Materiais, Laboratório de Processamento de Materiais Tecnológicos (LPMaT), Universidade Federal do Amazonas, Manaus, AM, Brazil

<sup>2</sup>Instituto Federal do Amazonas, Manaus, AM, Brazil

<sup>3</sup>Programa de Pós-Graduação em Física, Departamento de Física, Universidade Federal do Amazonas, Manaus, AM, Brazil

<sup>4</sup>Instituto de Pesquisas Energéticas e Nucleares, Cidade Universitária, São Paulo, SP, Brazil

<sup>5</sup>Pós-Graduação em Ciência e Engenharia dos Materiais, Universidade Federal do Piauí, Teresina, PI, Brazil

<sup>6</sup>Universidade Federal Rural de Pernambuco, Unidade Acadêmica do Cabo de Santo Agostinho, Cabo de Santo Agostinho, PE, Brazil

<sup>7</sup>Instituto de Desenvolvimento Tecnológico, Distrito Industrial I, Manaus, AM, Brazil

Received: 16 December 2022

Accepted: 21 January 2023

© The Author(s), under exclusive licence to Springer Science+Business Media, LLC, part of Springer Nature 2023

## ABSTRACT

In this work, the variation in the structural and electrical properties of lithium-doped sodium titanate, obtained from an ultrafast (15 min) microwave-assisted synthesis has been reported. X-ray diffraction and Rietveld analysis have been done to identify the present phases, their composition, and lattice parameters.  $\text{Na}_2\text{Ti}_3\text{O}_7$  was identified as the major phase, while  $\text{Na}_2\text{Ti}_6\text{O}_{13}$  was obtained as a secondary phase in all samples. The phase composition usually varies depending on the content of the doping element. In the sample with 0.5% lithium ions, an additional phase corresponding to  $\text{NaLiTi}_3\text{O}_7$  appeared. The microstructure of the ceramic samples showed an increase in the grains size and the appearance of small particles on the surface of the grains. This effect becomes more evident for the samples with 0.5% Li. Finally, the electrical properties of the ceramic samples studied were favored with an increase in doping and  $\sigma_{\text{dc}}$  values of  $1.94 \times 10^{-5} \text{ S cm}^{-1}$ ,  $2.51 \times 10^{-5} \text{ S cm}^{-1}$ , and  $4.00 \times 10^{-5} \text{ S cm}^{-1}$  were determined for  $\text{Na}_{2-x}\text{Li}_x\text{Ti}_3\text{O}_7$  with  $x = 0.0\%$ ,  $0.1\%$ ,  $0.5\%$  of  $\text{Li}^+$ .

Address correspondence to E-mail: yurileyet@yahoo.es

## 1 Introduction

Currently, the world is going through a new energy transition process, perhaps the most important from a climate point of view since the industrial revolution. In this context, the research for materials capable of generating and storing energy in a solid state is an area of strategic interest. The interest in solid-state batteries has been increasing due to their high durability, loading speeds, and energy density when compared with liquid ones. However, solid-state battery technology still needs to be improved before gaining market scale, requiring the replacement of rarer elements by more abundant species. Thus, sodium titanates have been widely studied in the past two decades due to their ion exchange capacity [1, 2]. With the chemical formula  $\text{Na}_2\text{Ti}_x\text{O}_{2x+1}$  ( $n = 3\text{--}8$ ), they have been reported for applications in photocatalysis [3], as adsorbents [4, 5], and in energy storage systems [6–11]. Sodium titanates have several crystalline phases [1, 2]. Between them, sodium trititanate ( $\text{Na}_2\text{Ti}_3\text{O}_7$ ) and sodium hexatitanate ( $\text{Na}_2\text{Ti}_6\text{O}_{13}$ ) have been highlighted due to their compelling electrical conductivity values, which are in the order of  $10^{-6} \text{ S cm}^{-1}$  [12–14].  $\text{Na}_2\text{Ti}_3\text{O}_7$  is a layered structure with a stacked  $\text{TiO}_6$  octahedral ribbon, while  $\text{Na}_2\text{Ti}_6\text{O}_{13}$  is a type of tunnel structure with a  $\text{TiO}_6$  octahedron that shares its edges [6, 7, 15]. The channels of the tunnel may help to elucidate the higher mobility of the active sodium vacancies that are demonstrated by sodium hexatitanate structures [2, 7, 16]. Although hexatitanate shows higher electrical conductivity, both phases might improve the ion exchange capacity. Wu et al. [7] reported the synergistic effect of  $\text{Na}_2\text{Ti}_3\text{O}_7$  and  $\text{Na}_2\text{Ti}_6\text{O}_{13}$  hybrid structures to enhance electrochemical performance when compared with isolated structures.

Sodium titanates have been reported as possible candidates to replace lithium as a material for batteries due to their similar physical and chemical properties [6–8, 17–24]. Despite the considerable similarity in sodium and lithium properties, previous experiments have shown that  $\text{Li}^+$  has greater diffusion capacity than  $\text{Na}^+$  and, consequently, higher electrical conductivity [8, 18, 19]. Therefore, many studies have been carried out to improve the electrical conductivity of sodium titanates, in particular,  $\text{Na}_2\text{Ti}_3\text{O}_7$  and  $\text{Na}_2\text{Ti}_6\text{O}_{13}$  [1, 20, 22].

To overcome this poor ion and electron conductivity, some studies have involved doping sodium

titanates, especially  $\text{Na}_2\text{Ti}_3\text{O}_7$  [25, 26]. For instance, Song et al. [20] carried out a self-doping of  $\text{Ti}^{3+}$  in the  $\text{Na}_2\text{Ti}_3\text{O}_7$  electrode material and confirmed that it exhibited a superior electrochemical performance than the non-doped  $\text{Na}_2\text{Ti}_3\text{O}_7$  electrode material. Xia et al. [22] synthesized  $\text{Na}_2\text{Ti}_3\text{O}_7$  doped with some elements of the lanthanides series and compared them with pure  $\text{Na}_2\text{Ti}_3\text{O}_7$ . All doped samples exhibited superior electrochemical performance for use as an electrode material. Pal et al. [15] synthesized lithium mixed sodium trititanates and reported that the conductivity increases as the concentration of lithium increases due to the accommodation of lithium and sodium ions in the interlayer space.

Several synthesis methods have been applied in order to synthesize sodium titanates, such as the use of solid-state reaction [8, 15–17], the sonochemical method [12, 14, 18], ball milling [2], sol-gel [19, 20], and microwave-assisted hydrothermal methods [6, 13]. Although all methods are effective, most of them have a longer synthesis time. For instance, Dynarowska et al. [8] used the solid-state method for 24 h and synthesized  $\text{Na}_2\text{Ti}_3\text{O}_7$  and  $\text{Na}_2\text{Ti}_6\text{O}_{13}$  as a secondary phase. Youssry et al. [2] used the ball milling method for 20 h and synthesized pure  $\text{Na}_2\text{Ti}_3\text{O}_7$  while Basilio et al. [13] used the microwave-assisted hydrothermal method for 1 and 4 h and synthesized  $\text{Na}_2\text{Ti}_3\text{O}_7$  as a major phase and  $\text{Na}_2\text{Ti}_6\text{O}_{13}$  as a secondary phase. The main objective of this work is to reveal the influence on the structural and electrical properties of lithium-doped sodium titanate, obtained by microwave-assisted ultrafast synthesis (15 min).

## 2 Experimental procedure

First, a solution composed of  $1 \text{ mol L}^{-1}$  sodium hydroxide ( $\text{NaOH}$ , Synth, purity > 98%), dissolved in deionized water, isopropyl alcohol ( $\text{C}_3\text{H}_8\text{O}$ , Synth), and titanium isopropoxide ( $\text{C}_{12}\text{H}_{28}\text{O}_4\text{Ti}$ , Sigma-Aldrich, 97%) was obtained. The titanium isopropoxide was diluted in isopropyl alcohol, and, in an ultrasonic bath, it was dripped into the  $\text{NaOH}$  solution. The mixture was maintained in the ultrasonic bath for 10 min. Subsequently, the precursors were placed in a microwave (Anton Paar, Multiwave 3000) under the parameters of 800 W for 15 min. The obtained powder was dried in an oven at  $110^\circ \text{C}$ , then

a portion of the material was heat-treated at 800 °C/1 h to induce crystallization [2].

For the synthesis of sodium titanates doped with lithium, fractions of NaOH were replaced by 1 mol L<sup>-1</sup> lithium acetate dihydrate (C<sub>2</sub>H<sub>3</sub>LiO<sub>2</sub>·2H<sub>2</sub>O, Sigma-Aldrich, 97%). The calculation of substitutional NaOH doping for C<sub>2</sub>H<sub>3</sub>LiO<sub>2</sub>·2H<sub>2</sub>O was performed in terms of molarity (1 and 5%) and converted into volumetric ratios considering the concentrations: 0.96 g/mL C<sub>12</sub>H<sub>28</sub>O<sub>4</sub>Ti, 0.040 g/mL for NaOH and 0.102 g/mL for C<sub>2</sub>H<sub>3</sub>LiO<sub>2</sub>·2H<sub>2</sub>O. The lithium-doped sodium titanate-doped samples were also heat-treated at 800 °C/1 h. The material heat-treated at 800 °C/1 h was compacted (150 MPa) into disc shape samples (2 mm thickness and 12 mm diameter) for 5 min. Then, the green samples were sintered at 850 °C for 1 h, using a muffle furnace without atmosphere control. These sintered samples will be called NLT0, NLT1, and NLT5, for  $x = 0.0\%$ ,  $0.1\%$ , and  $0.5\%$  depending on the lithium content, respectively.

The X-ray diffraction (XRD) was carried out in a diffractometer (Empyrean, Malvern Panalytical), in the interval (2 $\theta$ ) from 5° to 80°, using a copper tube as an x-ray source ( $k_{\alpha} = 1.5406$  Å), at 40 kV voltage and 40 mA. The structural refinement was performed using the Rietveld method and the Fullprof software [27].

The morphology was analyzed using scanning electron microscopy (VEGA3, TESCAN), equipped with a tungsten thermionic emission system, suitable for high and low vacuum operations.

The electrical characterization was carried out using the Complex Spectroscopy technique, in an impedance analyzer (Solartron 1260). Measurements were carried out at room temperature using a potential of 500 mV in a frequency ranging from 10 Hz to 1 MHz.

### 3 Results and discussion

Figure 1a–c shows the Rietveld refinement plot for all synthesized samples studied using the Fullprof software (2018). The quantitative phase analysis identified two monoclinic phases in the NLT0 sample (Fig. 1a): disodium trititanate - Na<sub>2</sub>Ti<sub>3</sub>O<sub>7</sub>, which exhibits the space group of P21/m (ICSD 25,000) and lattice parameters  $a$ ,  $b$ ,  $c$ , and  $\beta$  of 8.568(5) Å, 3.797(1) Å, 9.128(5), and 101.576° (6), respectively, as

illustrated in Table 1; sodium hexatitanate - Na<sub>2</sub>Ti<sub>6</sub>O<sub>13</sub>, with the space group of C2/m (ICSD 23,877) and lattice parameters of 15.088(2) Å, 3.750(5) Å, 9.164(1) Å, and 98.831° (1). The quantitative analysis for the NLT0 sample showed the existence of a majority phase (85.81±1.96 %) that corresponds to Na<sub>2</sub>Ti<sub>3</sub>O<sub>7</sub>. However, a secondary phase, which corresponds to Na<sub>2</sub>Ti<sub>6</sub>O<sub>13</sub> (14.19±1.09%) was also identified. The weight fraction of each phase and the statistical parameters of the refinement can be seen in Table 1.

Similar to what was found for sample NLT1, there are two polymorphs in their composition, as can be observed in Fig. 1b. The majority fraction (66.03±2.43 %) was reached for the Na<sub>2</sub>Ti<sub>3</sub>O<sub>7</sub> phase, therefore, indicating that the addition/insertion of 1 of Li<sup>+</sup> ions favors the increase (33.97±2.13% of the Na<sub>2</sub>Ti<sub>6</sub>O<sub>13</sub> phase content. Although there are two monoclinic structures, a third phase was found for the NLT5 sample (Fig. 1c). This corresponds to the orthorhombic structure of NaLiTi<sub>3</sub>O<sub>7</sub> with the space group of Cmca and lattice parameters  $a$ ,  $b$ , and  $c$  of 16.521(1), 11.215(1) Å, and 11.504(1) Å, respectively. For NTL5 the majority phase continuing to be Na<sub>2</sub>Ti<sub>3</sub>O<sub>7</sub>; however, this phase was 14% greater than that obtained for NLT1 and 6% less than the phase percentage obtained for NLT0.

Several factors can influence phase formation and concentration. One factor might be the introduction of doping. The Li-ion has an ionic radius of 0.92 Å for coordination with seven oxygen atoms [28]. This radius is small compared to the Na<sup>+</sup> ion of 1.12 Å and 1.24 Å in the coordination of seven and nine, respectively [28]. Therefore, one should expect a decrease in the lattice parameters when the Li-ion replaces the Na<sup>+</sup> ion in the crystal structure. The non-variation of the lattice parameters and the unit cell volume in Na<sub>2</sub>Ti<sub>3</sub>O<sub>7</sub> phases for the NLT1 and NLT5 samples indicates that the Li-ion enters an interstitial form in the structure. In the NLT5 sample, a decrease in the parameters  $a$ ,  $c$ , and  $\beta$  in Na<sub>2</sub>Ti<sub>6</sub>O<sub>13</sub> is observed. This suggests that the Li-ion replaced the Na ion in the Na<sub>2</sub>Ti<sub>6</sub>O<sub>13</sub> crystal structure. The appearance of the third phase NaLiTi<sub>3</sub>O<sub>7</sub> for the NLT5 sample indicates a solubility limit of the Li-ion within the Na<sub>2</sub>Ti<sub>6</sub>O<sub>13</sub> structure. Statistical parameters showed the result of Rietveld refinement (see Table 1).

To reaffirm the result discussed above, the cation-anion bond lengths and the distortion index of the Na-O oxygen polyhedrons were determined. For this, the atomic positions of the Na<sup>+</sup> and O<sup>2-</sup> ions in the

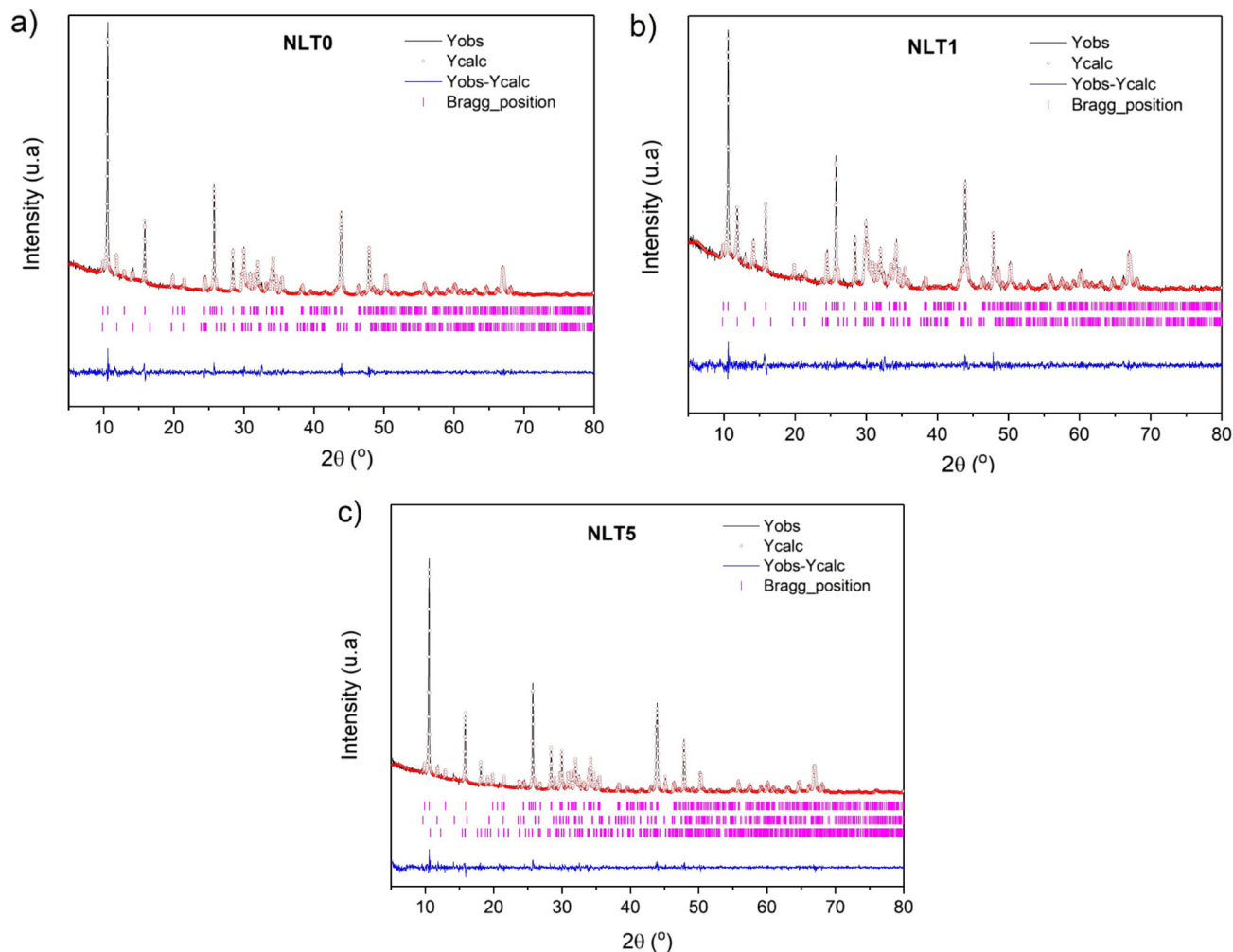


**Fig. 1** Rietveld refinement plot of the three studied samples, **a** NLT0, **b** NLT1, and **c** NLT5. Where NLT0, NLT1 and NLT5 = 0.0%, 0.1% and 0.5% lithium content, respectively. The identification of each line appears inserted in the upper part of the graph

$\text{Na}_2\text{Ti}_3\text{O}_7$ ,  $\text{Na}_2\text{Ti}_6\text{O}_{13}$ , and  $\text{NaLiTi}_3\text{O}_7$  phases were refined. The crystalline structures of the three phases were visualized using the VESTA software [29] and are shown in Fig. 2. Six Ti octahedrons and four Na polyhedrons with seven and nine oxygen anions are observed in the  $\text{Na}_2\text{Ti}_3\text{O}_7$  phase. Twelve Ti octahedrons and two equivalent Na polyhedrons are maintained in the  $\text{Na}_2\text{Ti}_6\text{O}_{13}$  phase. The values of the average bond length and the distortion index of the Na–O polyhedrons are shown in Table 2.

Table 2 shows that the distortion index in the NLT1 sample is below 1% in the Na–O polyhedrons in the  $\text{Na}_2\text{Ti}_3\text{O}_7$  and  $\text{Na}_2\text{Ti}_6\text{O}_{13}$  structures. In addition, the distortion index values of the Na–O polyhedrons are very close in the NLT0 and NLT1 samples. This suggests that the Li-ion introduces itself interstitially in both  $\text{Na}_2\text{Ti}_3\text{O}_7$  and  $\text{Na}_2\text{Ti}_6\text{O}_{13}$  structures for the

NLT1 sample, as a represented in Fig. 2. In the case of the NLT5 sample, the distortion index reached the value of 1.12% for Na–O oxygen polyhedrons in the  $\text{Na}_2\text{Ti}_6\text{O}_{13}$  structure, indicating an increase in the distortion and the possibility of a minor substitution of the  $\text{Na}^+$  by  $\text{Li}^+$  ion. The highest distortion value (1.75%) appears for the Li–O polyhedrons in the  $\text{NaLiTi}_3\text{O}_7$  structure. These results agree with the behavior of the lattice parameters and unit cell volume.

Figure 3 shows the images obtained by scanning electron microscopy for the NLT0, NLT1, and NLT5 samples. As can be observed in Fig. 3a, there are grains with elongated and homogeneous formats, which appear randomly in the entire image. This morphology has been reported quite frequently in the literature [13]. For NLT1 (Fig. 3b), a microstructure

**Table 1** Lattice parameters, phase composition, and refinement parameters

Sample	NLT0	NLT1	NLT5
Phase $\text{Na}_2\text{Ti}_3\text{O}_7$			
$a$ (Å)	8.568 (5)	8.564 (9)	8.566 (4)
$b$ (Å)	3.796 (1)	3.796 (4)	3.799 (2)
$c$ (Å)	9.128 (5)	9.125 (9)	9.127 (5)
$\beta$ (°)	101.58 (6)	101.57 (7)	101.59 (4)
$V$ (Å <sup>3</sup> )	290.8 (3)	290.5 (5)	290.9 (1)
$\rho$ (g/cm <sup>3</sup> )	3.443	3.528	3.442
% wt	85.81±1.96	66.03± 2.43	79.79±00.93
Phase $\text{Na}_2\text{Ti}_6\text{O}_{13}$			
$a$ (Å)	15.088 (2)	15.100 (2)	15.008 (6)
$b$ (Å)	3.750 (5)	3.747 (5)	3.752 (8)
$c$ (Å)	9.164 (1)	9.147 (2)	9.128 (8)
$\beta$ (°)	98.831 (1)	98.122 (14)	97.006 (7)
$V$ (Å <sup>3</sup> )	512.3 (1)	511.2 (2)	509.7 (5)
$\rho$ (g/cm <sup>3</sup> )	3.506	3.504	3.471
%wt	14.19±1.09	33.97± 2.13	10.15±00.78
Phase $\text{NaLiTi}_3\text{O}_7$			
$a$ (Å)			16.521 (1)
$b$ (Å)			11.215 (9)
$c$ (Å)			11.504 (10)
$V$ (Å <sup>3</sup> )			2131.55 (1)
$\rho$ (g/cm <sup>3</sup> )			3.557
%wt			10.07±0.10
Refinement parameters			
$R_{\text{wp}}$	7.99	7.42	8.37
$R_{\text{exp}}$	6.61	6.36	7.29
$\chi^2$	1.46	1.36	1.32

The errors of each magnitude are included. Where NLT0, NLT1, and NLT5 = 0.0%, 0.1%, and 0.5% lithium content, respectively

that is very similar to that seen in Fig. 3a can be seen; however, there is an increase in the agglomeration of the grains. Moreover, some regions can be observed with the presence of small particles on the surface of some grains. This small difference could be related to the introduction of  $\text{Li}^+$  ion into the sodium titanate structure. However, it is worth remembering that there were changes in the lattice parameters for this composition, as well as in the phase composition present in the material, which reinforces the possibility that these changes may indeed be motivated by the introduction of Li in the crystal structure of sodium titanate. Finally, in Fig. 3c, the presence of grains with shapes similar to those described above is observed, though covered with particles of smaller size and a different shape, which may be an important element to consider since it could be related to the increase in the amount of Li in the sodium titanate structure. Previously, using XRD, it was

observed that for this concentration of lithium ions, the sample presents the appearance of a new crystalline phase,  $\text{NaLiTi}_3\text{O}_7$ . Despite representing only 10% of the total crystalline phases present in the sample, this may be the reason for the changes in the morphological characteristics of the material.

Considering the structural and microstructural changes presented by the ceramic samples with different Li contents, it is of great interest to verify what happens from the point of view of electrical properties with this ceramic system. This study was performed using complex impedance spectroscopy as stated in the previous section. Figure 4a shows the Cole-Cole semicircles for the three samples under study. This graph shows the behavior of the imaginary part of the resistivity ( $\rho''$ ) as a function of the real part of the resistivity ( $\rho'$ ) and  $\rho^* = \rho' + i\rho''$ . It was clearly noted that as the  $\text{Li}^+$  ion content increases, the diameter of the semicircle of resistivity decreases. It



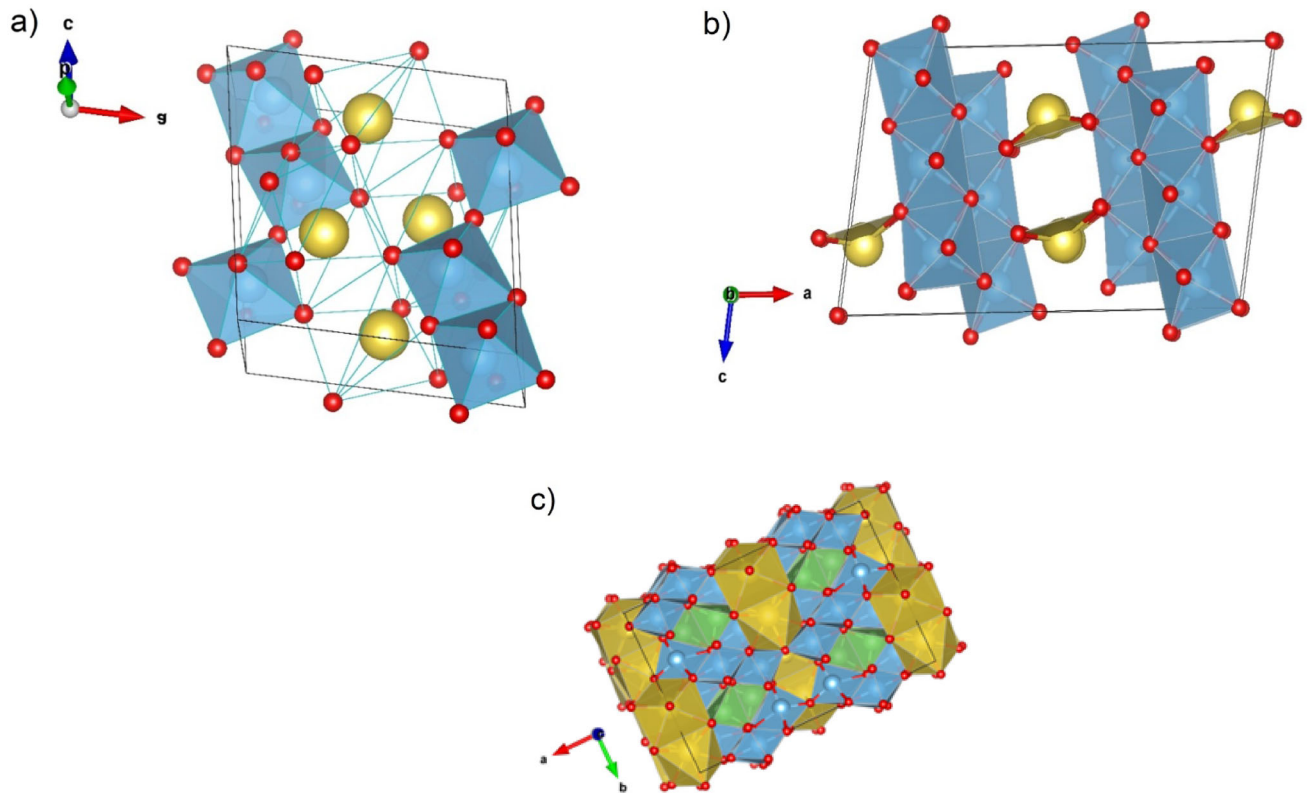


**Fig. 2** Visualization of the crystalline structures for **a**  $\text{Na}_2\text{Ti}_3\text{O}_7$ , **b**  $\text{Na}_2\text{Ti}_6\text{O}_{13}$ , and **c**  $\text{NaLiTi}_3\text{O}_7$ . In this figure, the red spheres represent oxygen atoms, the yellow ones are sodium atoms and the blue ones, titanium atoms

**Table 2** Values of the average bond length of Na–O, Ti–O, and Na–Ti, and the distortion index of the oxygen polyhedrons

Parameter	Bond	NLT0	NLT1	NLT5
$\text{Na}_2\text{Ti}_3\text{O}_7$				
Polyhedron average distance (Å)	Na1–O	2.72(1)	2.72(1)	2.72(1)
	Na2–O	2.56(1)	2.56(1)	2.56(1)
Distortion index (BL)%	Na1–O	0.74	0.89	0.84
	Na2–O	0.24	0.21	0.22
$\text{Na}_2\text{Ti}_6\text{O}_{13}$				
Polyhedron average distance (Å)	Na1–O	2.51(5)	2.58(2)	2.58 (1)
Distortion index (BL)%	Na1–O	0.68	0.63	1.12
$\text{NaLiTi}_3\text{O}_7$				
Polyhedron average distance (Å)	Na1–O			2.63(7)
	Na2–O			2.69(7)
	Li1–O			2.00(5)
Distortion index (BL)%	Na1–O			0.08
	Na2–O			0.92
	Li1–O			1. 75

Where NLT0, NLT1, and NLT5 = 0.0%, 0.1% and 0.5% lithium content, respectively

should be noted that the diameter of this semicircle is associated with the total resistivity of the samples, and in this case, the values were indicated inside the graph. It was verified that the NLT0 sample, with 0%

lithium ions in its structure, has the highest resistivity value (51  $\text{k}\Omega \text{ cm}$ ). The values reported here are at least one order of magnitude lower than those previously reported for ceramics materials with a similar

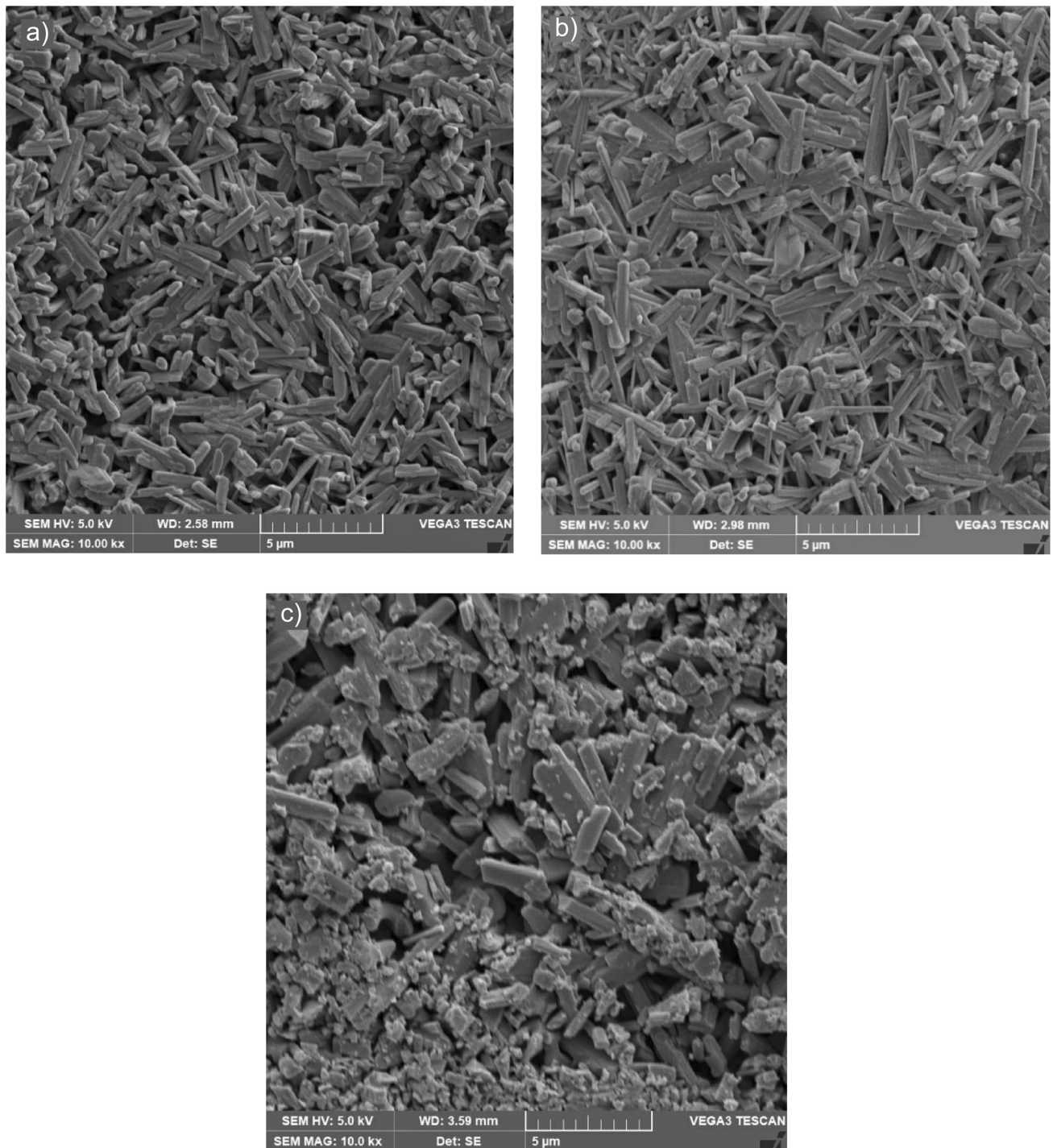


**Fig. 3** SEM image of the ceramic samples **a** NLT0, **b** NLT1, and **c** NT5. Where NLT0, NLT1, and NLT5 = 0.0%, 0.1%, and 0.5% lithium content, respectively

phase composition [13]. It's important to remember that the synthesis time in this work was only 15 min. In the case of reference [13], the synthesis times were 1 and 4 h, respectively.

As can be seen with the increase in lithium content in the samples, there is a decrease in the diameter of the semicircles. This behavior is associated with a decrease in the resistance of the samples. The total resistivity values obtained for each sample were 51

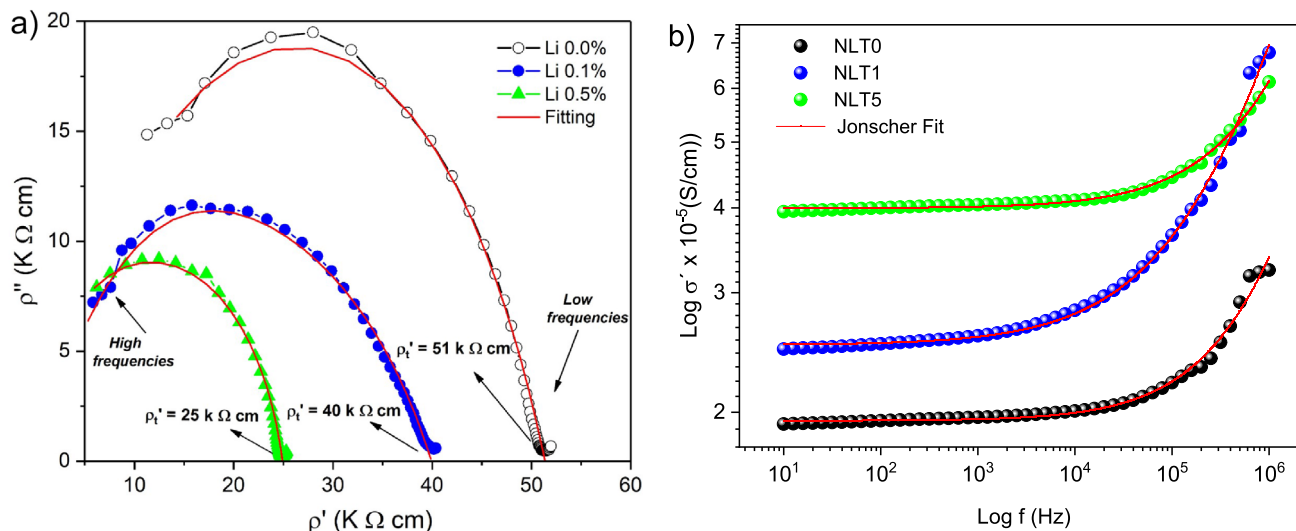


**Fig. 4** **a** Cole-Cole diagram with symbols for the different samples in the study. **b** Relation between AC conduction and the measurement frequency. The solid red lines represent the

$K\Omega$  cm,  $40 K\Omega$  cm and  $25 K\Omega$  cm for the samples NLT0, NLT1, and NLT5, with 0.0, 0.1, and 0.5% of lithium, respectively. It is possible to note that NLT5 presented the lowest resistivity value compared to the other samples. This fact is probably linked with the minor presence of  $\text{Na}_2\text{Ti}_6\text{O}_{13}$ . Usually in the literature this phase is reported to have poor performance in the electrical conductivity [30]. In addition, this phase (in sample NLT5) presents lower  $\beta$  (o) and higher distortion index (BL). Then, it may have differentiated electronic properties. The minor content of  $\text{Na}_2\text{Ti}_6\text{O}_{13}$  is partly compensated by the obtaining the phase  $\text{NaLiTi}_3\text{O}_7$ , which increases the ionic mobility [31].

A simple and very useful way to determine the DC conductivity is by using the Jonscher equation [32]. This allows us to study the dependence of the AC conductivity with frequency and considers the so-called universal response, which is associated with the total DC conductivity in the region of low frequencies:

$$\sigma'(f) = \sigma_0 \left[ 1 + \left( \frac{f}{f_0} \right)^n \right]$$

Where  $\sigma_0$ ,  $f$  and  $f_0$  are the DC conductivity, the linear frequency, and the frequency at which dispersion begins, respectively. Meanwhile,  $n$  represents the exponential parameters, with values between 0 and 1.

Figure 4b presents the behavior of AC conductivity as a function of frequency; the solid lines represent

adjustment made by the equivalent circuit in graph (a) and the adjustment following the Jonscher equation (b) NLT0, NLT1, and NLT5 = 0.0%, 0.1%, and 0.5% lithium content, respectively

the adjustment following the Jonscher equation. In this figure, it can be seen that the three samples show similar behavior, though with different values. The values of DC conductivity were determined for each sample. In all cases, the adjustment error was less than 3.5%. As expected, the highest conductivity value corresponded to the sample with the highest concentration of lithium ions, namely NLT5 ( $4.00 \times 10^{-5} \text{ S cm}^{-1}$ ). The NLT1 sample corresponded to a value of  $2.51 \times 10^{-5} \text{ S cm}^{-1}$ . While the pure sample NLT0 presented the lowest value of DC conductivity, which was  $1.94 \times 10^{-5} \text{ S cm}^{-1}$ . These results are in agreement with what was discussed and presented previously herein. There are not many reports in the literature regarding the samples presented here, and this makes a direct comparison of these results difficult. However, Hongzheng Zhu et al. [33] presented an extensive study and various materials with potential application in solid-state electrolytes, and reported DC conductivity values of between  $10^{-4} \text{ S cm}^{-1}$  and  $10^{-6} \text{ S cm}^{-1}$ , which are similar to those reported herein. Martinez-Cisneros et al. [34] reported DC conductivity values of between  $10^{-3} \text{ S cm}^{-1}$  and  $10^{-5} \text{ S cm}^{-1}$  for NASICON materials; however, these were for applications in liquid electrolytes. These results can be considered a possible route for a new generation of materials with potential application in solid-state electrolytes, and which can be obtained simply and quickly. However, more conclusive studies are still required.



## 4 Conclusion

The lithium effect on the structural and electrical properties of  $\text{Na}_{x-1}\text{Li}_x\text{Ti}_3\text{O}_7$  ceramics produced in a short period of time (15 min) using the microwave method were investigated. It was verified by XRD and Rietveld analyzes that lithium induces a variation in the composition of the phases ( $\text{Na}_2\text{Ti}_3\text{O}_7$  and  $\text{Na}_2\text{Ti}_6\text{O}_{13}$ ) present in all ceramics. For the NLT5 sample, the appearance of a major crystalline phase corresponding to  $\text{NaLiTi}_3\text{O}_7$  and lower presence of  $\text{Na}_2\text{Ti}_6\text{O}_{13}$  was detected. The SEM images presented samples with similar grain formats, which increase and become covered with smaller particles with the increase in lithium content. From the electrical point of view, it was shown that with the introduction of the dopant, an improvement in the conductivity of the samples occurs. The highest value of DC conductivity was  $4.00 \times 10^{-5} \text{ S cm}^{-1}$  and corresponded to NLT5. Finally, it can be said that this is a fast synthesis route and that the materials obtained here present good DC conduction properties, making them possible candidates for solid-state electrolytes.

## Acknowledgements

This study was financed in part by the “Coordenação de Aperfeiçoamento de Pessoal de Nível Superior - Brasil (CAPES)” - Finance Code 001. The authors would like to thank “Fundação de Amparo à Pesquisa do Estado do Amazonas” and “Conselho Nacional de Desenvolvimento Científico e Tecnológico” for their financial support.

## Author contributions

All authors contributed with the study and design, as well as the materials preparation and data collection, and analysis that were performed. All authors read and approved the final manuscript.

## Data availability

The datasets generated during the current study are available from the corresponding author on reasonable request. Compliance with Ethical Standards.

## Declarations

**Conflict of interest** The authors declare that there are no competing financial interests and also they have no known competing financial interests or personal relationships that influence the work reported in this work.

## References

1. J.P. Da Silva et al., *J. Alloys Compd.* **867**, 159025 (2021)
2. M. Youssry, A. Mussa, *Ceram. Int.* **47**, 14021–14032 (2021)
3. Y.C. Chang, J.C. Lin, S.H. Wu, *J. Alloys Compd.* **749**, 955–960 (2018)
4. M. Zhao et al., *Environ. Pollut.* **248**, 938–946 (2019)
5. J. Reyes-Miranda, A. Garcia-Murillo, A. Garrido-Hernández, F. de Carrillo-Romo, *J. Mater. Lett.* **292**, 129589 (2021)
6. O. Cech et al., *J. Energy Storage* **14**, 391–398 (2017)
7. C. Wu et al., *Adv. Sci.* **5**, 1800519 (2018)
8. M. Dynarowska, J. Kotwiński, M. Leszczynska, M. Marzantowicz, F. Krok, *Solid State Ion.* (2017). <https://doi.org/10.1021/cm202076g>
9. H. Zhu et al., *J. Electroanal. Chem.* **788**, 203–209 (2017)
10. Y. Liu, Z. Wang, L. Gao, L. Zhang, X. Yang, *Mater. Lett.* **291**, 129602 (2021)
11. S. Chandel et al., *J. Electroanal. Chem.* **877**, 114747 (2020)
12. N.G. Fagundes et al., *Solid State Sci.* **88**, 63–66 (2019)
13. L.A.L. Basilio et al., *Ceram. Int.* **46**, 23834–23839 (2020)
14. L. Aguilera et al., *Ceram. Int.* **46**, 8706–8710 (2020)
15. D. Pal, R.K. Pal, J.L. Pandey, S.H. Abdi, A.K. Agnihotri, *J. Mater. Sci. Mater. Electron.* **21**, 1181–1185 (2010)
16. P. Li et al., *Electrochim. Acta* **187**, 46–54 (2016)
17. H. Pan et al., *Adv. Energy Mater.* **3**, 1186–1194 (2013)
18. Y. Leyet et al., *J. Solid State Electrochem.* **22**, 1315–1319 (2018)
19. M. Zukalová et al., *J. Solid State Electrochem.* **22**, 2545–2552 (2018)
20. T. Song, S. Ye, H. Liu, Y.G. Wang, *J. Alloys Compd.* **767**, 820–828 (2018)
21. Y. Xu et al., *J. Power Sources* **408**, 28–37 (2018)
22. J. Xia et al., *Chem. Sci.* **9**, 3421–3425 (2018)
23. Z. Chen et al., *Materials (Basel)* **11**, 2206 (2018)
24. O. Cech, P. Vanysek, L. Chladil, K. Castkova 17th International Conference Advanced Batteries, Accumulators and Fuel Cells (Abaf 2016). vol.74, (2016) pp. 331–337
25. Y. Shi et al., *Electrochim. Acta* **321**, 134714 (2019)
26. J. Chen, X. Zhou, C. Mei, J. Xu, C.P. Wong, *Electrochim. Acta* **224**, 446–451 (2017)
27. J. Rodríguez-Carvajal, *Phys. B Phys. Condens. Matter.* **192**, 55–69 (1993)
28. R.D. Shannon, *Acta Crystallogr. Sect. A* **32**, 751–767 (1976)

29. K. Momma, F. Izumi, *J. Appl. Crystallogr.* **44**, 1272–1276 (2011)
30. X. Han, X. Gui, W. Tao, X. Li, T.F. Yi, *Ceram. Int.* **44**, 12273–12281 (2018)
31. M. Vadivazhagan, R. Jayan, K. Nallathamby, *Energy Fuels* **36**(2), 1081–1090 (2022)
32. A. Langar, N. Sdiri, H. Elhouichet, M. Ferid, *Results Phys.* **7**, 1022–1029 (2017)
33. H. Zhu, J. Liu, *J. Power Sources* **391**, 10–25 (2018)
34. C.S. Martínez-Cisneros et al., *J. Eur. Ceram. Soc.* **41**, 7723–7733 (2021)

**Publisher's Note** Springer Nature remains neutral with regard to jurisdictional claims in published maps and institutional affiliations.

Springer Nature or its licensor (e.g. a society or other partner) holds exclusive rights to this article under a publishing agreement with the author(s) or other rightsholder(s); author self-archiving of the accepted manuscript version of this article is solely governed by the terms of such publishing agreement and applicable law.